Journal of Structural Geology 30 (2008) 1242–1253

Contents lists available at ScienceDirect

Journal of Structural Geology

journal homepage: www.elsevier.com/locate/jsg

Micromechanisms of shear zone propagation at the brittle–viscous transition

F. Fusseis [a,b,*], M.R. Handy [b]

[a] School of Earth and Geographical Sciences, The University of Western Australia, Perth, Australia
[b] Department of Earth Sciences, Freie Universität Berlin, Germany

ARTICLE INFO

Article history:
Received 29 April 2007
Received in revised form 19 May 2008
Accepted 6 June 2008
Available online 27 June 2008

Keywords:
Shear zones
Shear zone propagation
Strain localization
Brittle-Ductile
Brittle-Viscous
Cap de Creus

ABSTRACT

Our investigation of progressively strained rock samples from the margins of greenschist-facies shear zones utilizes a space-for-time approach to reveal how the mylonitic overprint of metapsammitic and -pelitic host rocks at the Cap de Creus involved brittle fracturing. We present a set of microscale observations indicating that microfractures formed immediately prior to or coevally with a fine-grained mylonite. Microfracturing dominated early stages of strain localization on the scale of the shear zones. On the microscale, centimeter-long fractures facilitated strain softening by allowing enhanced fluid access, thereby accelerating the dynamic recrystallization of quartz and a metamorphic reaction of biotite. As these two processes produce a polyphase matrix of small, dislocation-poor grains that eventually form an interconnected, rheologically weak phase, fractures become inactive. This represents a strain-dependent brittle–viscous transition. We outline this transition in a conceptual model for the rheological evolution of mid-crustal shear zones.

1. Introduction

Heterogeneous deformation at greenschist-facies metamorphic conditions involves the formation of shear zones in which a mechanically weaker foliated rock, a mylonite, is formed (e.g., Ramsay, 1980; Means, 1984, 1995; Hull, 1988). Where this happens, a strain gradient across shear zones can be used to reconstruct the evolution of a mylonite in time (Hull, 1988; Mitra, 1984; Means, 1995). This assumption, that space can be used as a proxy for time, was applied by several authors to investigate the evolution of brittle and ductile shear zones (e.g., Mitra, 1979, 1984; Means, 1984; Ingles, 1986; Watterson, 1986; Hull, 1988; Carreras, 2001; Fusseis et al., 2006). The space-for-time assumption also reflects on the way strain gradients can be interpreted in terms of the rheological history of shear zones. Means (1984) classified shear zones based on their softening/hardening evolution. He distinguished Type 1 shear zones that harden with time and therefore widen as it gets easier to deform host rock than to keep on deforming the mylonite, from Type 2 shear zones that soften and progressively reduce their actively deforming width. The space-for-time proxy is only valid for Type 2 shear zones.

The space-for-time proxy is perfectly applicable to shear zone terminations where new host rock is continuously strained during shear zone propagation. Consequently, such terminations have been studied to understand strain localization in greenschist-facies mylonitic[1] shear zones (e.g., Ramsay and Allison, 1979; Simpson, 1983; Segall and Pollard, 1983; Segall and Simpson, 1986; Buergmann and Pollard, 1992; Tourigny and Tremblay, 1997; Guermani and Pennacchioni, 1998; Pennacchioni, 2005; Mancktelow and Pennacchioni, 2005). With a few exceptions, most of these authors describe fractures at the tips of the mylonitic shear zones with orientations that usually are parallel to the shearing plane. Due to their close proximity to the shear zone tips, such fractures were generally interpreted to have influenced the formation of the shear zones.

The timing of fracture formation with respect to mylonitic shearing differs in most authors' interpretations. For example, Segall and Simpson (1986) interpret fractures in their model to be reactivated remnants of earlier deformation phases. In contrast, Mancktelow and Pennacchioni (2005) argue that localized fracturing might have been immediately precursory to ductile strain localization. The significance of the time span between fracture formation and mylonitic shearing becomes clear when the micromechanisms of strain localization are to be reconstructed. While earlier, reactivated fractures and veins represent mechanical heterogeneities that concentrate stress and thus focus mylonitic overprint, fracturing as an integral part of mylonitic shear zone formation involves some sort of a microscale brittle-to-viscous transition. Few studies investigated the microstructural evolution of this transition in great

* Corresponding author. School of Earth and Geographical Sciences, The University of Western Australia, M004, 35 Stirling Highway, Perth, Australia. Tel.: +61 864882680.
E-mail address: florian@fusseis.at (F. Fusseis).

[1] Mylonitic deformation is accommodated by thermally activated, viscous creep mechanisms (Schmid and Handy, 1991).

0191-8141/$ – see front matter © 2008 Elsevier Ltd. All rights reserved.
doi:10.1016/j.jsg.2008.06.005

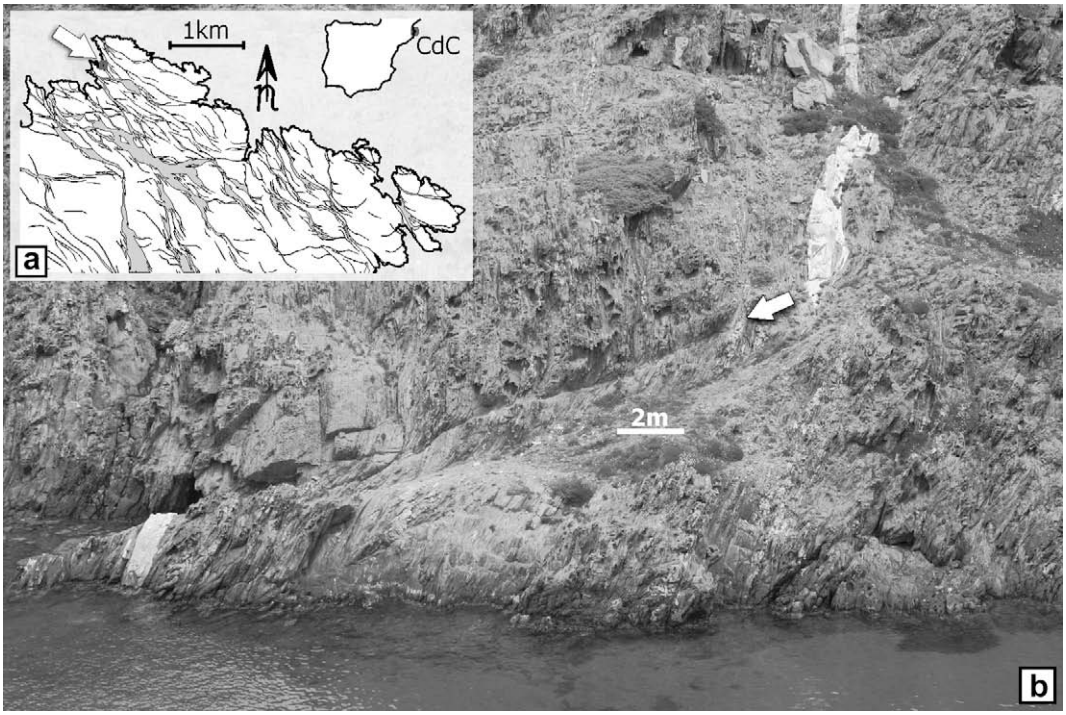

Fig. 1. (a) Location of the investigated area (arrow) within the Northern Shear Belt at the Cap de Creus peninsula (modified after Carreras, 2001); (b) Shear zone termination mapped in Fig. 2. UTM 31T 521678 east, 4687224 north, view across the Cala Prona towards the ENE.

detail, and it remains unclear exactly what grain scale processes interact as the brittle–viscous transition occurs.

In this study, which investigates greenschist-facies shear zones from the northern Cap de Creus peninsula in NE Spain, we extend our own, recently published studies of a strain-dependent brittle–viscous transition on the outcrop scale (Fusseis et al., 2006; Schrank et al., in press) to the microscale. We show how microfracturing relates to the temperature-activated deformation mechanisms during this transition. We demonstrate that during strain localization deformation is partitioned among the different mechanisms and discuss how the rheology of greenschist-facies shear zones evolves with strain and time.

2. Geological background and outcrop-scale observations

The shear zones of the Cap de Creus area (Figs. 1 and 2) formed during the retrograde evolution of a low-pressure/high-temperature metamorphism (peak metamorphic conditions 670 °C/470 MPa) associated with the Variscan orogenesis (Druguet, 2001 and references therein). The shear zones investigated in this study are exposed in the Cala Prona and Cala Serena areas along the northern shoreline of the peninsula (Fig. 1). They are hosted by a monotonous series of metamorphic pelitic and psammitic sediments composed of varying amounts of quartz (Qtz,[2] see Appendix for rock compositions), biotite (Bt), feldspar (mostly plagioclase Plag, An 20–35%), muscovite (Ms) as well as accessory chlorite (Chl), ilmenite (Ilm), tourmaline and epidote. Alternating pelitic and psammitic layers in these rocks (defining S0) are between a few centimeters to several meters thick and usually have sharp boundaries.

At least two deformation phases (D1 and D2) at prograde and peak metamorphic conditions affected these sediments prior to shear zone formation (Druguet, 2001; Carreras, 2001). During these deformational events S0 was tightly folded and sheared and a composite foliation (S0/2) formed (remnants of S1 could not be identified, Figs. 1, 2 and 12). On the microscale, S0/2 is characterized by generally well-aligned Bt^I (Fig. 3). In metapsammitic samples with Bt contents of up to 30%, Bt^I is dispersed and forms a continuous foliation (Fig. 3). With increasing mica content Bt^I appears clustered and organized in cleavage domains, which may be several hundred microns wide and alternate with microlithons[3] consisting of Qtz^I and $Plag^I$. In metapelites with Bt contents of up to 50%, cleavage domains may be several millimeters wide and form an interconnected network.

The shear zones investigated below formed in a statically annealed rock during retrograde cooling from about 550° to below 300 °C at lithostatic pressures of about 250 MPa (*D3 deformation event*, Carreras et al., 1977; Carreras and Garcia-Celma, 1982; Garcia-Celma, 1983; Druguet, 2001). D3 shear zones are characterized by a mylonitic foliation, S3, and a pronounced mineral lineation, L3. D3 shear zones are oriented at high angles to S0/2 (Figs. 1 and 2).

At the margins of the shear zones, S0/2 is bent (forming marginal drags) and gradually transformed into S3 (Fig. 2, Carreras and Garcia-Celma, 1982; Garcıa-Celma, 1983; Carreras, 2001). Bent S0/2 also forms monoclinal ductile beads ahead of shear zone tips (Elliott, 1976). In Fusseis et al. (2006) we concluded that the marginal drags were formed as shear zones propagated through these ductile beads. Based on the detailed shear strain evolution of the shear zone shown in Figs. 1 and 2, we classified D3 shear zones as Type 2 (softening) shear zones in the sense of Means (1984; see also fig. 5 in Fusseis et al., 2006). During increasing displacement, deformation was progressively concentrated in the narrow shear zone center and the marginal drags became inactive. Following Hull (1988) and Means (1995),

[2] Mineral abbreviations follow Bucher and Frey (1994). Supplementary roman numbering of these abbreviations refers to the generations of these minerals (e.g., Qtz^I – quartz, first generation).

[3] Sensu Passchier and Trouw, 2005.

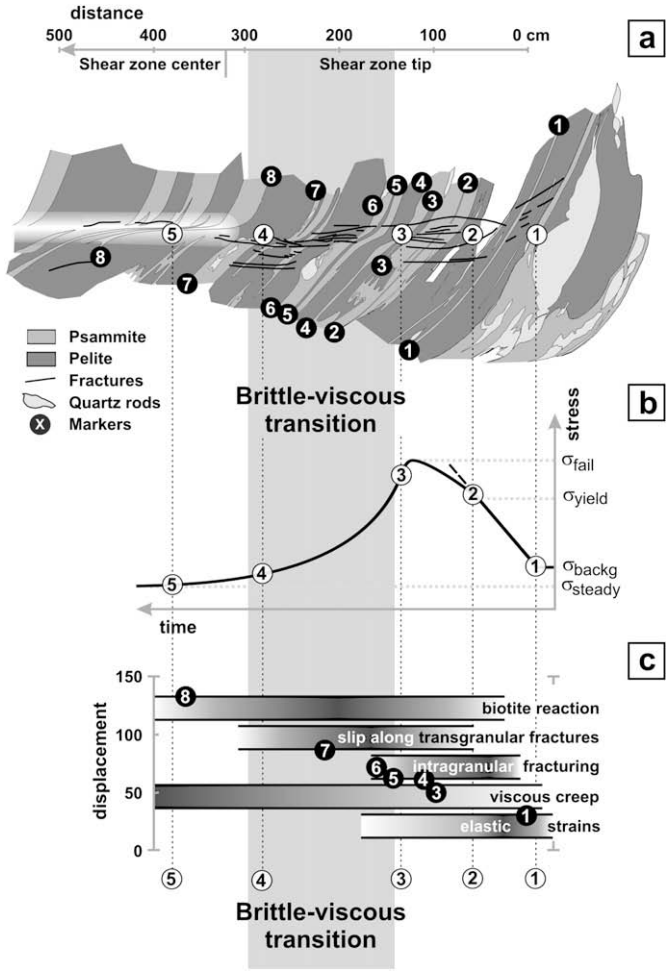

Fig. 2. (a) Termination of a mylonitic shear zone in the Cala Prona (see text for explanation). The shear zone is mapped approximately parallel to the stretching lineation and perpendicular to the mylonitic foliation, view to the ENE. (b) and (c): Model for the rheological evolution of the mylonite in the Cala Proba shear zone. (b) Inferred evolution of rock strength across the shear zone tip. White labels correspond to positions within the shear zone termination as shown in (a). (c) Qualitative estimate of activity (indicated by length of bars) and contribution (grey shading in bars, darker is relatively higher contribution) of various strain energy dissipating mechanisms with respect to accumulating displacement. Displacement as measured from markers in (a) on left ordinate. See text for explanation.

this justifies interpreting the microstructural evolution across marginal drags and ductile beads as representing a progressive evolution in time.

Based on field observations, we concluded that the formation of D3 shear zones involved a precursory stage of fracturing (Fig. 3) transitional with increasing strain to mylonitic flow (Fusseis et al., 2006). Fractures characterize low-strain segments of shear zones (i.e., their marginal drags and tips), where they formed subparallel to the later mylonitic shearing plane and show the same sense of shear as the later mylonitic shear zones. Strain at the tips of shear zones is partitioned into slip on these fractures and viscous folding of the existing foliation S0/2 forming the ductile bead ("shear zone tip" in Fig. 2a, figures 10 and 11 in Fusseis et al., 2006). In high-strain parts of mylonitic shear zones, deformation is entirely accommodated within the narrow viscously deforming shear zone center, where no fractures occur (Fig. 2a, figure 5 in Fusseis et al., 2006). The tip and central parts of the shear zone are separated by a brittle-to-viscous transition (Fig. 2).

In the following we describe the microstructures associated with this transition as documented in metapsammitic, metapelitic

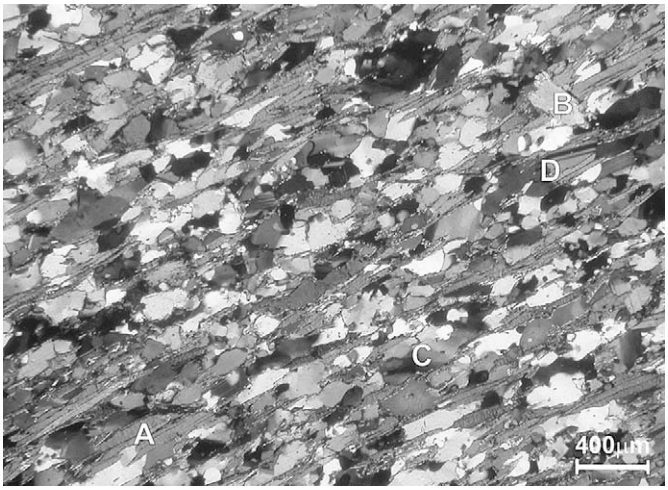

Fig. 3. Sample CC05 showing the background strain recorded by the host rock. S0/2 in the sample is defined by aligned Bt1 ('A'). Ms overgrowing S0/2 ('B') postdates this deformation. The sample exhibits a minor D3 mylonitic overprint: Bt shows reaction rims, Qtz ('C') exhibits minor undulatory extinction and dynamic recrystallization, Plag shows polysynthetic deformation twins ('D'). Crossed polarizers, XZ sections.

and Qtz-vein samples that were collected at the tips and in the marginal drags of several mylonitic shear zones in the Cala Serena and Cala Prona area (see Fig. 2 and Appendix for sample locations and sample descriptions). The samples show a progressive reduction in grain size from the host rocks to the mylonitic shear zone centers. Progressive grain size reduction is generally interpreted to be associated with strain softening behaviour (White et al., 1980; Poirer, 1980), which justifies the application of the space-for-time proxy. This allows us to use differently strained samples collected at different distances from the centers of the mylonitic shear zones to reconstruct the progressive evolution of the shear zones (Fig. 2, Mitra, 1984; Hull, 1988; Means, 1995).

3. Microstructures at the tips of mylonitic shear zones

D3 deformation caused a bulk dynamic overprint of the rocks, resulting in minor undulatory extinction, minor grain boundary bulging and few subgrains in Qtz^{I} as well as narrow reaction rims around Bt^{I}, where Bt^{II} and Ilm formed (Fig. 3, Garcıa-Celma, 1983). Shearing beyond this background strain resulted in the formation of a fine-grained mylonite, whose proportion increases across the margins towards the centers of the shear zones. The observations from progressively deformed samples presented below indicate that dynamic recrystallization, pressure solution, neocrystallization and microfracturing were active during D3 shearing. Microstructures indicative of at least two of these deformation mechanisms were identified in all of the samples, evidencing that the mechanisms operated coevally. It therefore stands to reason that strain, during the mylonitic overprint, was partitioned among these deformation mechanisms. However, as will be shown, the relative importance and contribution of the individual processes varied in dependence of strain.

3.1. Distributed heterogeneous shearing

The intensity of the mylonitic overprint generally increases across marginal drags and the ductile beads towards the shear zone center. This overprint involves deformation of the main constituent minerals Qtz^{I} and Bt^{I} and, to a minor degree, of $Plag^{I}$ and Ms^{I}. The

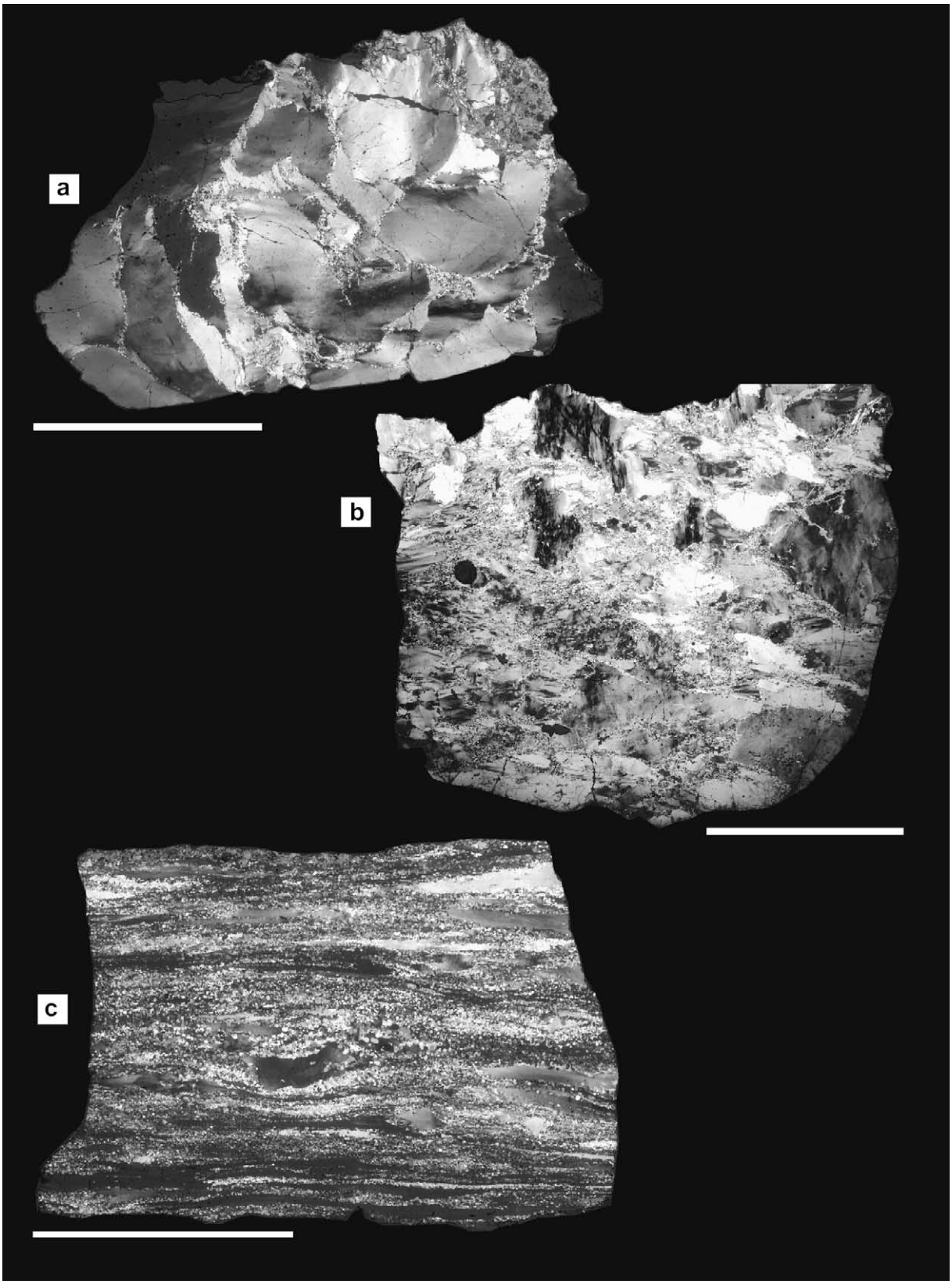

Fig. 4. Series of progressively deformed quartz samples (CC33) from a vein dragged into a D3 shear zone. Dynamic recrystallization is dominated by grain boundary migration and subgrain rotation. (a) Qtz^{I} grains with undulatory extinction and mantles of small ($\sim$50 μm) dynamically recrystallized Qtz^{II}. Sample CC33c. (b) Increasing proportion of Qtz^{II} grains. Sample CC33d. (c) Highly strained quartz vein, remnant Qtz^{II} ribbon grains. Sample CC33b. Scale bar is 10 mm in all pictures. Crossed polarizers, XZ sections.

latter two never form interconnected layers and are therefore interpreted not to have influenced the rheology of the rocks.

Dynamic overprint of Qtz^{I} commences by the formation of sweeping undulatory extinction (Fig. 4a). Between Qtz^{I} grains, which can be up to several millimeters in diameter, mantles of small (<100 μm) dynamically recrystallized Qtz^{II} grains form by grain boundary bulging recrystallization (Fig. 4a, 'B' in Fig. 5a). In higher strained samples these mantles become thicker and replace the relict Qtz^{I} grains (Fig. 4b). Subgrain boundaries form within Qtz^{I}, transecting entire grains (Fig. 5b). Intermediately to highly strained quartz-rich samples exhibit Qtz^{I} ribbons and high proportions of dynamically recrystallized Qtz^{II} grains (Fig. 4c). In samples from the centers of mylonitic shear zone, all Qtz^{I} has been replaced by fine-grained Qtz^{II} (grain size ~80 μm, table 5.3 in Fusseis, 2006).

Bt^{I} deforms by basal glide, pressure solution and minor kinking, all of which are typical deformation mechanisms for biotite at greenschist-facies conditions (Fig. 6a, e.g., Kerrich et al., 1980, 1981; Shea and Kronenberg, 1992, 1993). Along pressure solution seams, kink bands and at its grain boundaries, *brown* Bt^{I} has fine-grained (20–50 μm) mantles consisting of *green* Bt^{II}, Ms^{II}, Ilm, and Chl (Fig. 6). Such newly crystallized seams occur also in unsheared host-rock samples. However, they are more common in samples from shear zone margins. Kerrich et al. (1980, 1981) as well as Barnett and Kerrich (1980) have described similar fabrics as reaction fabrics ($Bt^{I} \rightarrow Bt^{II} + Ms^{II} + Chl + Ilm$), reflecting a tendency of biotite to reduce its Ti-content and adjust its Mg/(Mg + Fe) ratio accordingly during retrograde cooling (Henry and Guidotti, 2002; Henry et al., 2005).

The proportion of newly crystallized reaction products increases towards the center of the shear zone. In low-strain samples (Fig. 6b and c) the recrystallized grains form an interlocked and undeformed matrix with grain sizes <100 μm. Towards the shear zone center and with increasing shear strain, reaction products in the matrix become aligned parallel to S3 (Fig. 11).

Samples from mylonitic shear zone centers (i.e., more than 300 cm from the shear zone tip in Fig. 2) are characterized by a mixture of very fine grains (<50 μm) dominated by Qtz^{II} and Bt^{II} with clasts of Fsp and Ms (Fig. 11). The fine grain size of these ultramylonites (<100 μm) and their polyphase composition in combination with a heterogeneous phase distribution suggest that grain size-sensitive diffusion creep accommodated some of the imposed strain (Fig. 11, e.g., Fitz Gerald and Stunitz, 1993; Stunitz and Fitz Gerald, 1993; Newman et al., 1999).

3.2. Localized heterogeneous shearing

3.2.1. Intragranular microfractures

Microfractures and their healed remnants, fluid inclusion planes (FIPs, Anders and Wiltschko, 1994; Lespinasse, 1999; Boullier, 1999) are common features in samples from the external parts of shear zone margins, especially in quartz. FIPs are clearly more frequently found in Qtz^{I} (i.e., >500 μm) grains (Fig. 7a), however, relatively shorter segments were found transecting smaller grains in dynamically recrystallized domains of Qtz^{II} (Fig. 7b). FIPs in Qtz^{I} grains often terminate within the grain, and where they extend to grain boundaries they can occasionally be traced into the neighboring grains (arrow in Fig. 7b). In Qtz^{II} domains they tend to terminate at grain boundaries but were not found to transect them (Fig. 7b). Instead we found FIPs continued as trails of fluid inclusions along adjacent grain boundaries (Fig. 7c and d). Within domains of Qtz^{II} grains we identified many smaller inclusions decorating randomly oriented grain boundaries (Fig. 7e). In some cases, FIPs appear deflected across subgrain boundaries in Qtz^{I} (Fig. 7f). We interpret all of these observations to indicate that at least some FIPs were affected by dynamic recrystallization and thus formed prior to the onset of dynamic recovery. Even though most quartz samples contain several crosscutting generations of intragranular FIPs, most FIPs are orientated at high angles (<90°) to S1/2.

Microfractures and FIPs occur ahead of and parallel to isolated trains of dynamically recrystallized Qtz^{II} grains or subgrains in otherwise less deformed parental Qtz^{I} grains (Figs. 8 and 9a) and therefore seem associated with sites of pronounced dynamic recovery. Most grains forming these trains are roughly equidimensional and are smaller than subgrains in the host grains (Figs. 8 and 9a). The boundaries between the trains and the host grains are jagged and uneven. The trains are isolated from other subgrains in the host and tend to have markedly different crystallographic orientations compared to their parental grains ('B' in Fig. 8b, arrows Fig. 9a). They are often found where transgranular microshears crosscut Qtz^{I} (see next section).

That microfracturing predated or occurred coevally with dynamic recovery is evidenced by sample (CC14), where, in a bridge domain between two transgranular fractures, intragranular microfractures transect a Qtz^{I} grain (1–1′ and 2–2′ in Fig. 9a). Sweeping undulatory extinction in the segmented grain terminates against the microfractures ('A' in Fig. 9a), with the microfractures acting as obstacles to migrating dislocations.

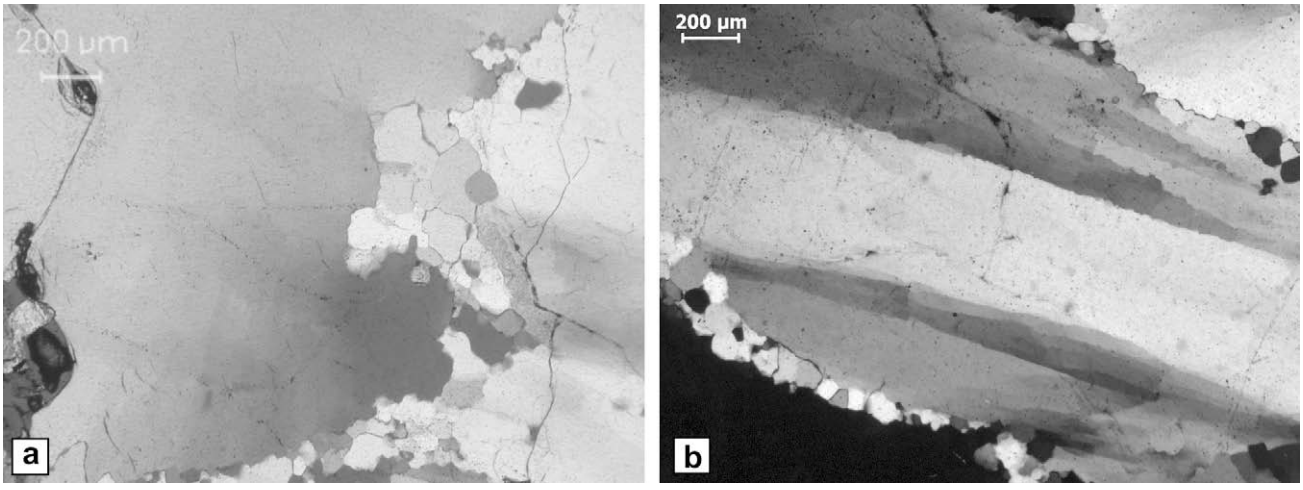

Fig. 5. Fluid inclusion planes (FIPs), dynamic recrystallization and healed microshears in series of a progressively deformed quartz samples (CC11). (a) Bulging Qtz^{I} grain boundary decorated by a mantle of dynamically recrystallized Qtz^{II} grains. Qtz^{I} grains exhibit FIPs (center of image). Sample CC11a. (b) Qtz^{I} grain segmented by subgrain boundaries. Marginally the grain exhibits bulges into the neighboring grains. Sample CC11b. Crossed polarizers, XY-sections.

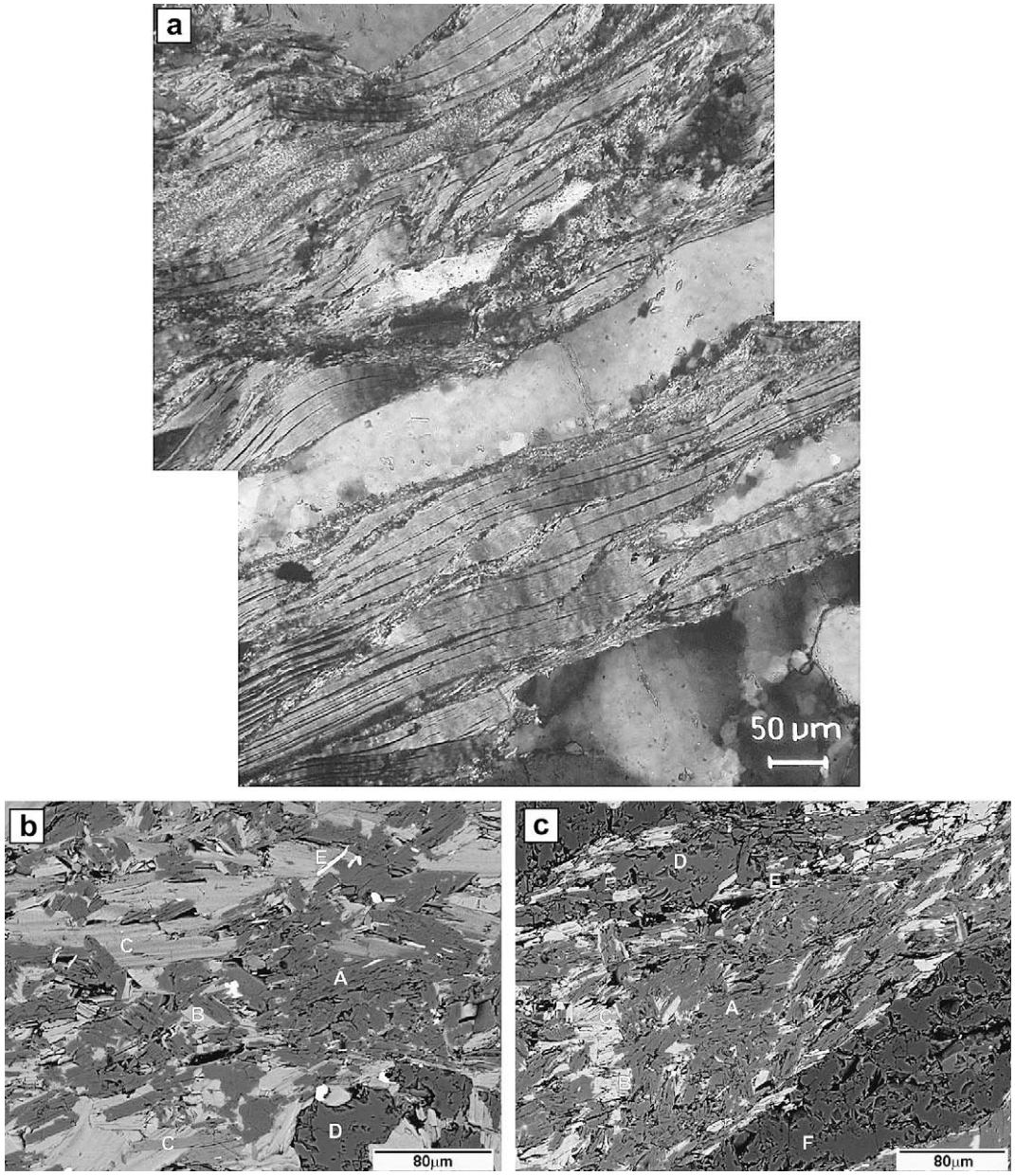

Fig. 6. (a) Bt deformation in sample CC17a. Bt deformed predominantly by basal glide, bending and pressure solution. Neocrystallized mantles consist of BtII, MsII, Ilm and Chl. Note Qtz ribbon between the two Bt aggregates. See text for explanation. Crossed polarizers, XZ section. (b, c) BSE images of fine-grained, undeformed aggregates of neocrystallized minerals in sample CC08 consisting of BtII, MsII, Ilm, Chl and minor Plag. Recrystallized phases (except Qtz and Plag) probably result from deformation-induced decay of BtI. 'A' – Ms, 'B' – Bt, 'C' – Chl, 'D' – Plag, 'E' – Ilm, 'F' – Qtz. See text for explanation. XZ section.

3.2.2. *Transgranular microfractures*

Towards the centers of mylonitic shear zones, microfractures occur as transgranular microshears some 2–3 cm long. They are generally parallel to decimeter-long shear fractures in the outcrop (and thus to S3) and truncate pre-existing microfabrics (Fig. 2a). Microshears more than 1 mm long and up to ~200 µm wide often occur in longitudinal arrays (1–1′ and 2–2′ in Fig. 9a). They displace grain boundaries (e.g., Ilm-trail displaced by microshear 3–3′ in Fig. 9b) and tend to crosscut S0/2 at angles between 30° and 80° (Fig. 9, S0/2 indicated by aligned Bt^{I}). In mica-rich samples, transgranular microshears evolve into shear bands with marginal drags. Evidence that transgranular microshears form by the interconnection of intragranular fractures is found in the observation that FIPs occur parallel to the terminations of microshears: Fig. 9b shows FIPs ('C' in Fig. 9b) in a Plag parallel to a transgranular microshear (1–1′ in Fig. 9b, same microshear as 1–1′ in Fig. 9a).

The microshears contain thin seams of a polymineralic fault rock with Bt^{II}, Ms^{II}, Ilm, minor secondary Chl and Qtz^{II} and $Plag^{II}$ in variable amounts (Fig. 10). These seams are hardly resolvable with the unaided eye and hence not visible in the field. Minerals are distributed heterogeneously in this fault rock (Fig. 10). The grain size increases abruptly from the microshears to their host minerals and the boundaries between fault rock and the host minerals are jagged and interpenetrating (Fig. 10c). Grains in microshears are between 30 and 150 µm in size and thus generally smaller than subgrains in dynamically recrystallized host grains and about two orders of magnitude smaller than the host grains themselves (Figs. 9a and 10b–d). All tabular or columnar minerals in the microshears are aligned parallel to their

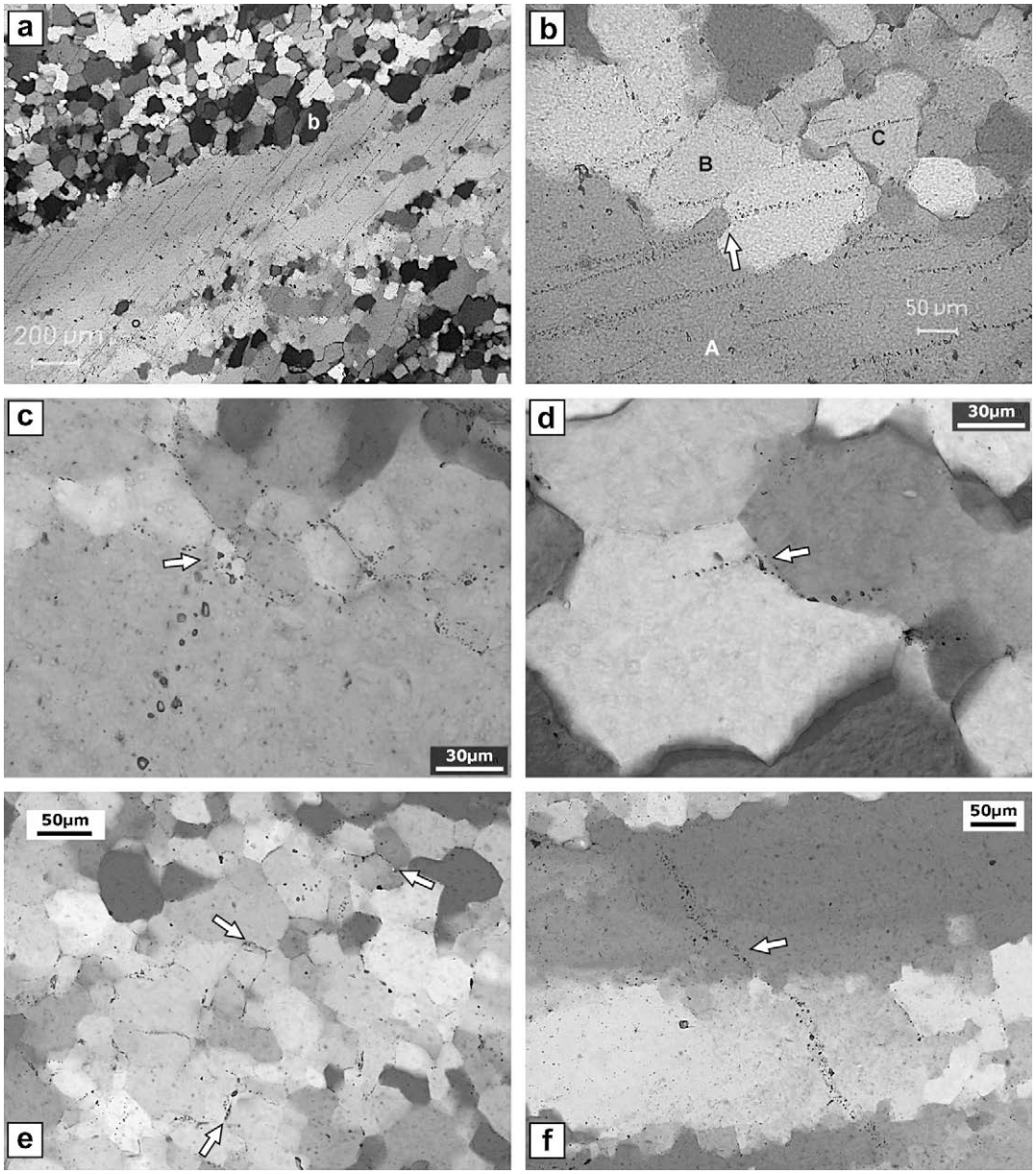

Fig. 7. (a) FIPs in a Qtz^{I} ribbon grain terminating against a domain of dynamically recrystallized Qtz^{II} grains (top half of the picture). Sample CC11c. (b) Boundary between a Qtz^{I} ribbon grain ('A') and a domain of Qtz^{II} grains ('B', 'b' in (a)). Short segments of FIPs are preserved in the Qtz^{II} grains immediately neighboring the Qtz^{I} grain. Sample CC11c. (c) FIP in quartz terminating against a grain boundary (arrow). Grain boundaries adjacent to the arrow are decorated with smaller fluid inclusions. Sample CC33e. (d) FIP in quartz deflected into a grain boundary (arrow). Sample CC11c. (e) Grain boundaries in a Qtz^{II} domain being decorated by small fluid inclusions (arrows) Sample CC33e. (f) FIP deflected by crystal-plastic deformation of a Qtz^{I} grain. Sample CC33e. Crossed polarizers, b–f with gypsum plate inserted. XZ sections.

boundaries (Fig. 10b and d). The formation of the polymineralic fault rock is ambiguous (see Section 4). Yet, all of the minerals described along the transgranular microshears are clearly second-generation, which indicates syntectonic nucleation and growth in the microshears.

4. Interpretation and discussion

4.1. The relationship between microfracturing, viscous creep and neocrystallization

A crucial assumption for the model of the strain-dependent brittle–viscous transition at the Cap de Creus shear zones is that planar discontinuities mapped at shear zone terminations formed as brittle fractures, as proposed by Fusseis et al. (2006). The following interpretations of the microstructural observations presented above support this model and indicate that fracturing occurred prior to or during the mylonitic overprinting and strain localization.

Crosscutting relationships between fluid inclusion planes and dynamically recrystallized grains of Qtz^{I} reveal the relative timing of fracturing and dislocation creep. The fact that short segments of FIPs often terminate at grain boundaries in Qtz^{II} domains (which consist of Qtz^{II}- and remant Qtz^{I} grains) but were not found to transect them (Fig. 7b) suggests that fluids from inclusion planes in Qtz^{I} grains were redistributed during dynamic recrystallization. A number of authors suggested the possible drainage of fluid inclusions by migrating grain boundaries; they proposed that migration is enhanced by the release of fluids into these boundaries (Kerrich, 1976; Wilkins and Barkas, 1978; Urai, 1983; Urai et al.,

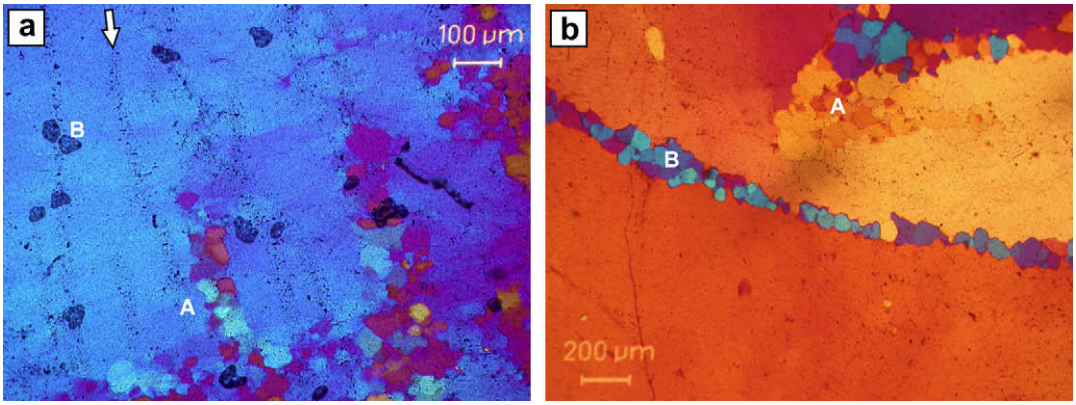

Fig. 8. FIPs, dynamic recrystallization and healed microshears in a series of progressively deformed quartz samples (CC11). (a) Subparallel FIPs and array of dynamically recrystallized Qtz^{II} grains ('A'). 'B' are air bubbles resulting from sample preparation. Sample CC33e. (b) Qtz^{I} grain partly dynamically recrystallized by subgrain rotation ('A'). Array of recrystallized Qtz^{II} grains within the host grain shows a systematic difference in crystallographic orientation ('B'). Sample CC11b. Crossed polarizers with gypsum plate inserted. XZ sections.

1986; Bakker and Jansen, 1990, 1994). Fig. 7f also indicates that fluid inclusion planes were affected by progressive lattice misorientation (subgrain rotation) during dynamic recovery. These observations indicate that fluid inclusions already existed during dynamic recovery and recrystallization and hence, that fracturing occurred prior to the mylonitic overprint of Qtz^{I}.

Another important observation in this context is the spatial association of fluid inclusion planes and isolated trains of Qtz^{II}

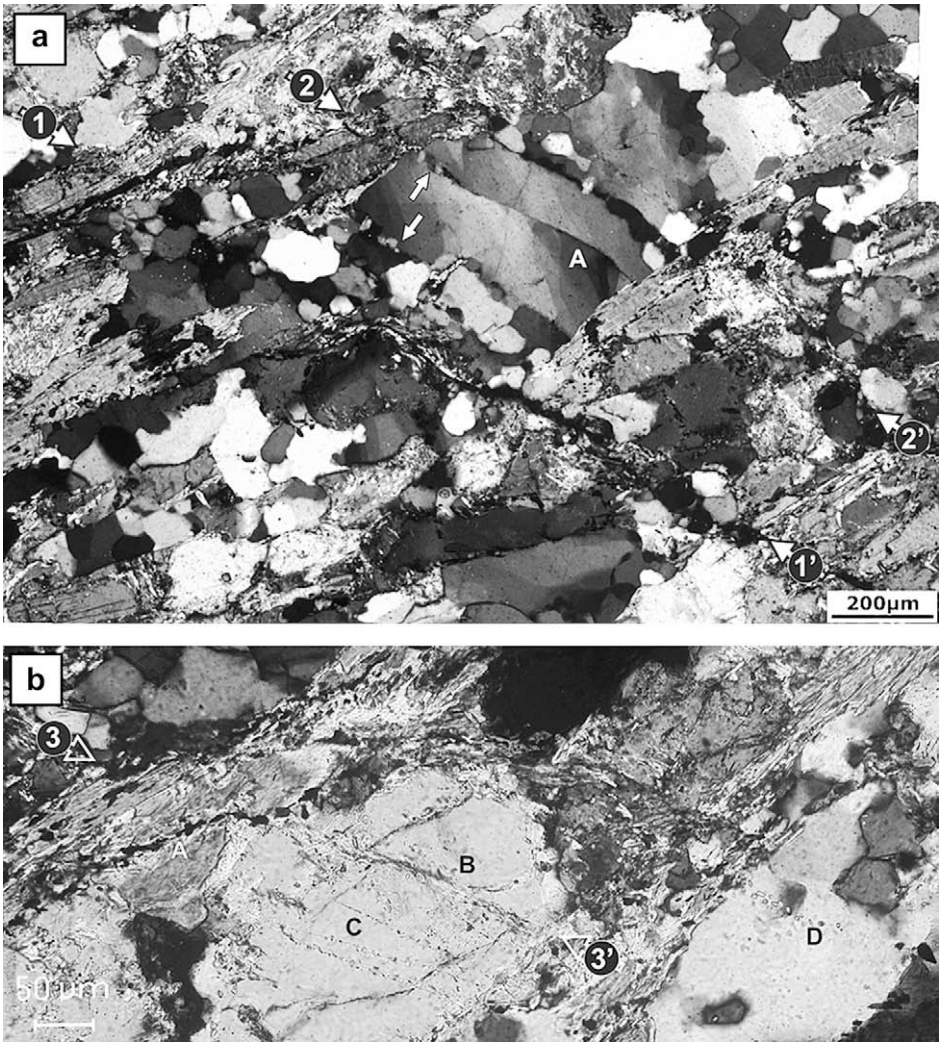

Fig. 9. Transgranular microshears (a) Contractional stepover between two microshears (1–1' and 2–2'). Note intragranular microfractures and recrystallized grains in central Qtz-microlithon ('A' and arrows). (c) Microshear (3–3') crosscutting Bt, Plag and Qtz grains. Note displaced Ilm-trail ('A'), small mica in microshear plane ('B'), FIPs ('C') and crystallized inclusions ('D'). Crossed polarizers, XZ section. Sample CC14.

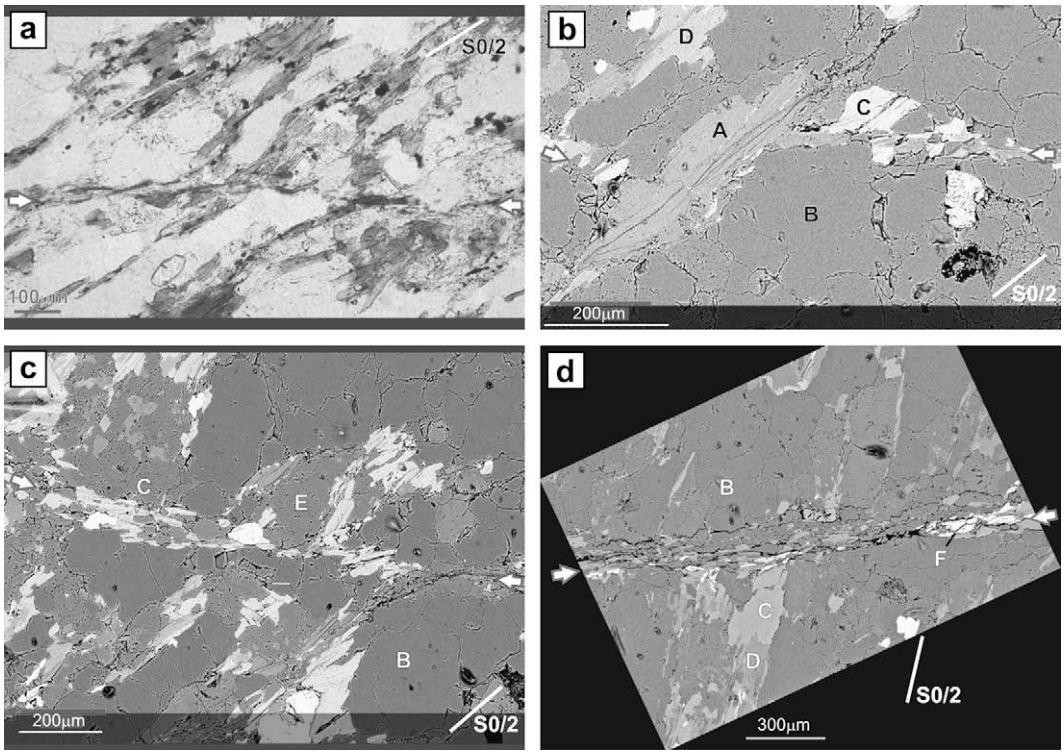

Fig. 10. Transgranular microshears (indicated by white arrows) from sample CC37. (a) Microshear transecting S0/2. Note alignment of dynamically recrystallized minerals in the microshear. (b) Microshear offsetting the left margin of an Ms porphyroclast aligned within S0/2 ('A'). Note the small dynamically recrystallized minerals defining the microshear. 'B' – Qtz, 'C' – Bt, 'D' – Chl. BSE image. (c) Transgranular microshear defined by aligned Bt, equigranular Qtz and Plag ('E', otherwise labeling as in (b)). BSE image. (d) Transgranular microshear crosscutting S0/2. Labeling as in (b), 'F' – Ilm. BSE Image.

grains *within* Qtz^{I} hosts (Fig. 8). Where fluid inclusion planes occur in the prolongation of the trains (e.g., Fig. 8a), no conclusion about the relative timing of fracturing, fluid infiltration and dynamic recrystallization can be drawn. Fractures may have formed (subcritically?) and healed at the tips of already existing and deforming trains, with the weak and dislocation-poor Qtz^{II} grains acting as stress concentrators (e.g., Atkinson and Meredith, 1986; Brantley, 1992). On the other hand, fluid inclusions may have posed obstacles to dislocation movement and subgrain walls might have formed due to pinning of dislocations at FIPs (White, 1976, 1977; Urai et al., 1986; Drury and Urai, 1990).

The trains themselves are a hint to a solution of this problem. Their formation is somewhat ambiguous and several possibilities need to be discussed. An evolution by progressive subgrain rotation can be excluded, because clearly no host-control misorientation relationship between old and new grains exists (Fig. 8, e.g., Ji and Mainprice, 1988; Kruse et al., 2001; Stunitz et al., 2003). Alternatively, the bulging of microcracks may have been responsible for dynamic recrystallization at sites of earlier microfracturing, as demonstrated by Urai (1983). Yet, bulging cannot explain the often significant misorientation of the dynamically recrystallized grains with respect to both adjacent parts of the host crystal (Fig. 8b), because grains resulting from bulging recrystallization generally inherit the crystallographic orientation of their parental grain (e.g., Stipp et al., 2002).

A third explanation overcomes these limitations: in a number of experimental studies in quartz and feldspar, cataclasis was described as being related to the formation of subgrains (Fitz Gerald et al., 1991; van Daalen et al., 1999; McLaren and Pryer, 2001; Stunitz et al., 2003; Vernooij et al., 2006; Trepmann et al., 2007; Nyman et al., 1992 described similar mechanisms from amphibole). To explain the formation of microshears, these authors employ a model that involves the interaction and interconnection of propagating microfractures, rigid-body rotation and subsequent dynamic recrystallization. Strain localization is initiated by dislocation tangles that concentrate stress. Stress rises until the yield strength of quartz is reached whereupon microcracks form and propagate. Shearing along these microcracks crushes quartz between them and individualizes new grains as the crystal fragments rotate passively. These grains then recrystallize in the presence of an aqueous fluid to form the observed planar trains. The model involves a close temporal and spatial link between fracturing, the formation of fluid inclusion planes and crystal-plastic deformation. It also clearly entails that fracturing and dislocation creep were not simply superposed but interacted with and were dependent on each other.

This model combines two processes (fracturing, viscous creep) that generally operate on different time-scales. However, brittle fracturing at the given retrograde, greenschist-facies conditions most likely involves a fracture mechanism called high-temperature cleavage (*Cleavage 3* of Ghandi and Ashby, 1979; Atkinson, 1982). Characteristic for Cleavage 3 fractures are general crystal-plastic strains of the deforming minerals of up to 10% preceding fracture formation (Ghandi and Ashby, 1979). At greenschist-facies conditions a significant amount of the fracture propagation can be expected to happen subcritically in the presence of an aqueous fluid, crack growth being stabilized and slowed down by accelerated crystal plasticity in the tip regions of the cracks (Kirby and McCormick, 1979; Tullis and Yund, 1980; Atkinson and Meredith, 1986; McLaren et al., 1989; Paterson, 1989). Thereby viscous and brittle deformation rates may converge.

The polyphase fault rock in the transgranular microshears is another microstructural feature indicating that fractures formed at greenschist-facies temperatures. It can be best explained by a combination of brittle fragmentation, recrystallization and mineral growth in existent microshears. A late (post-mylonitic)

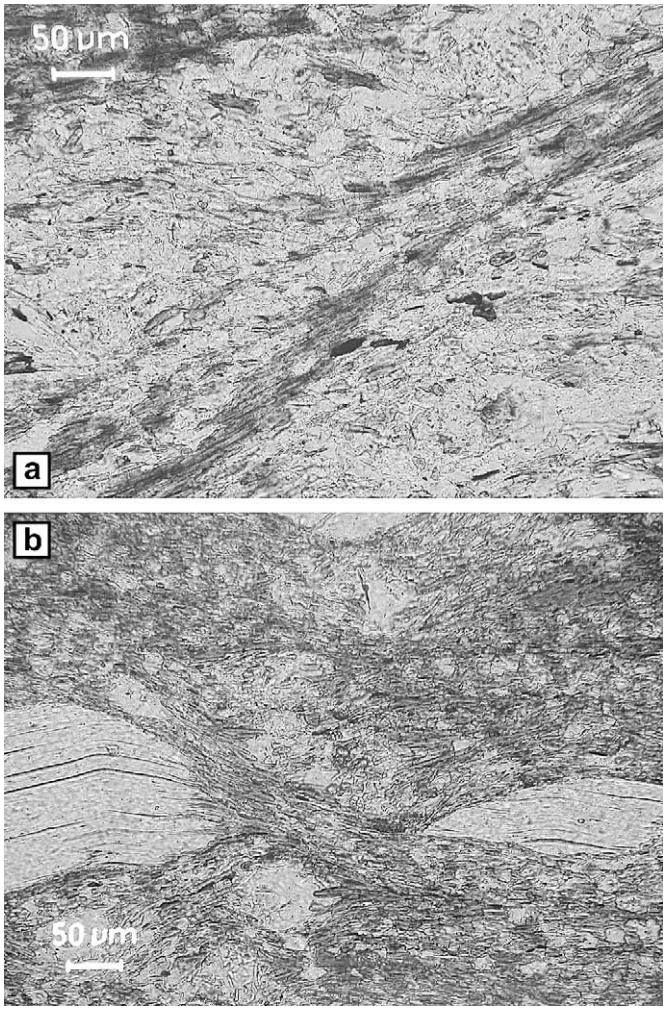

Fig. 11. Mylonitic microfabrics (a) Sample CC01, showing a top-to-south east shear band in S3. Bt^{II} is aligned within the shear band. (b) Sample CC52. Boudinaged Ms^{I} porphyroclast with fringes of green Bt^{II} forming in the boudin necks. Note small, uniform grain size of synmylonitic minerals. Both micrographs plane polarizers, XZ sections.

cataclastic origin seems unlikely, even though cataclasis and granular flow might explain the occurrence and distribution of Qtz^{II} and $Plag^{II}$ in the microshears. However, the jagged boundaries, which the minerals in the microshears have towards their host minerals indicate static, diffusion-assisted healing at elevated temperatures after mineral fragmentation (Fig. 10). Greenschist-facies temperatures are also suitable for the nucleation of the Bt^{II}, Ms^{II}, Ilm and Chl in the microshears as greenschist-facies products from the breakdown of Bt^{I} (Kerrich et al., 1980, 1981; Barnett and Kerrich, 1980). The alignment of the phases nucleated in this way can be explained either by granular flow after nucleation (March, 1932) or by mylonitic shearing after their growth (cf. Simpson, 1986). However, these observations clearly indicate that the transgranular microshears themselves already existed when the greenschist-facies mineral assemblage formed in them.

4.2. The interaction of brittle and viscous mechanisms during shear zone propagation

The interpretations of the microstructures described above can be combined in a conceptual model for the rheological and microstructural evolution of the brittle-to-viscous transition in quartz-rich rocks at greenschist-facies conditions. Utilizing the space-for-time assumption we illustrated this model in Fig. 2b and c for the tip of the shear zone where most of the samples for this study were collected (see Figs. 2 and 12). In this model, rock strength is inferred to evolve progressively with the evolving microstructures, i.e., across the process zone (Fig. 2b). The undeformed host rock ahead of the propagating shear zone is considered relatively 'strong', but the rock is expected to weaken ultimately as a mylonite forms (Fig. 2b). Mylonite formation involves coeval intra- and transgranular fracturing, dislocation creep and reaction of biotite. Across the process zone, the relative contribution of these microscale mechanisms varies with increasing strain (Fig. 2c). To illustrate the *qualitatively-estimated* relative contributions of individual processes we used color shading, following Herwegh and Handy (1996), with black indicating the greatest possible contribution of a given mechanism.

The host rock ahead of shear zone tip is stressed to a background level (σ_{back}) which is accommodated mainly by elastic strain (Fig 2b). σ_{back} may reach the yield strength of individual minerals, triggering the production and migration of dislocations. Dislocation tangling is only partly counteracted by the annihilation of dislocations at existing grain boundaries and by very limited grain boundary migration and subgrain formation (Fig. 3). Work hardening causes stress to rise at the outermost margins of the shear zone ('1' in Fig. 2). Stress concentrations at tangled dislocations may locally exceed the fracture strength of Qtz^{I} and $Plag^{I}$, causing the formation and subcritical propagation of intragranular

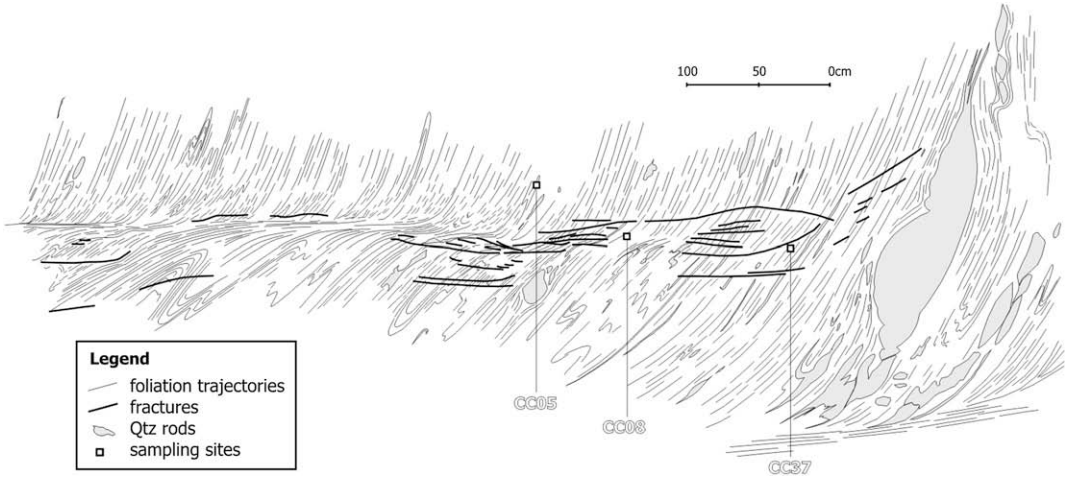

Fig. 12. Foliation trajectory sketch map of tip of shear zone shown in Figs. 1 and 2 with sampling locations of samples CC08, CC08, CC37.

microfractures (Fig. 2c). At the same time, dynamic recovery commences, causing grain boundaries to migrate and dislocations to polygonize and form subgrains (subsumed under 'viscous creep' in Fig. 2c). The rate of work hardening decreases ('2' in Fig. 2) as the lengths and number of microfractures increase (σ_{yield} in Fig. 2b). Crystal-plastic deformation blunts smaller microcracks, whereas some intragranular fractures propagate across grain boundaries and interconnect to form transgranular microshears (Figs. 2c and 9). They appear as fractures on the outcrop scale and their formation marks the peak strength of the rock (σ_{fail} in Fig. 2b). A considerable amount of displacement is then accommodated by slip along transgranular microshears (Fig. 2a).

By creating effective pathways for fluids, transgranular fractures influence the rheological evolution of the rock at this stage. Fluids not only decrease effective normal stresses on fracture surfaces and ease frictional sliding, but also accelerate the reaction of biotite ('2' in Fig. 2) by providing an agent. At the same time, quartz weakens hydrolytically, enhancing dynamic recrystallization (e.g., McLaren et al., 1989; Kohlstedt, 2006). Both processes, the reaction of biotite and the dynamic recrystallization of quartz, produce small dislocation-free and therefore weaker grains (Figs. 4 and 6, e.g., White et al., 1980). The proportion of these grains increases with increasing displacement in the shear zone (Figs. 4 and 7). This stage marks the brittle–viscous transition at a critical shear strain of $\gamma \sim 1$ (calculated over the entire width of the shear zone, '3'–'4' in Fig. 2). As the percentage of dynamically recrystallized and newly grown fine-grained minerals increases, fractures accommodate a smaller proportion of the bulk strain ('4' in Fig. 2). Few microfractures form at this stage and fault rock in microshears recrystallizes dynamically (Fig. 10).

At higher shear strains all quartz grains are dynamically recrystallized and most primary biotite has reacted (Figs. 4c and 11). Dislocation creep and grain size-sensitive diffusion creep replace fracturing as the dominant (i.e., strength-controlling) deformation mechanism (Figs. 2c and 11). The strength of the mylonite evolves gradually towards a stable value (σ_{stead}) as steady-state microfabrics form ('5' in Figs. 2b and 11).

5. Conclusions

We present microstructural observations that indicate how microfracturing contributed, through a strain-dependent brittle–viscous transition, to the formation of a viscously deforming mylonite at greenschist-facies conditions. By utilizing a space-for-time approach we identify brittle and viscous microscale processes involved in strain softening and link them in a conceptual model for the rheological evolution of shear zones in the middle crust. Our study is a first step towards an integrated understanding of strain energy dissipating processes during strain localization at crustal depth corresponding to the brittle–viscous transition. Our future investigations will attempt to systematically quantify these contributions.

Acknowledgements

We enjoyed stimulating discussions with Claudio Rosenberg, Matthias Konrad-Schmolke, Christoph Schrank, Patience Cowie, Neil Mancktelow, Holger Stunitz and Klaus Regenauer-Lieb and thank Jordi Carreras for his kind assistance throughout this project. We furthermore thank Elena Druguet and an anonymous reviewer for their useful and constructive criticism. We acknowledge the permit issued by the Cap de Creus national park authorities for collecting rock samples. Our work was supported by the German Science Foundation (DFG, grant Ha 2403/6), by the FU-Berlin and the University of Western Australia in Perth.

Appendix

Average rock compositions

Metapsammites (based on point-count analysis of 9 thin sections): Qtz: 45.3%, Bt: 28.2%, Fsp (mostly plag, An 20–35%): 18.5%, Ms: 4.3%, accessory Chl, Ilm, tourmaline, epidote.

Metapelites (point-count analysis of 5 thin sections): Qtz: 36.4%, Bt: 37.6%, Fsp: 18.6%, Ms: 4.2%, accessory Chl, Ilm, tourmaline, epidote.

Sample compositions and sampling locations

CC01 Metapsammite (44.6% quartz, 24.1% biotite, 15.4% plagioclase, 9.8% muscovite, 4.0% opaque undefined ore phase, accessory epidote, tourmaline). Cala Prona, UTM 31T 521678 east, 4687224 north. Collected from the center of the mylonitic shear zone in Fig. 2, about 16 m NW of the shear zone termination (cf. figure 5 in Fusseis et al., 2006).

CC05 Metapsammite (48.8% quartz, 30.6% biotite, 7.6% plagioclase, 5.4% muscovite, 4.8% k-feldspar, accessory epidote, tourmaline). Cala Prona, UTM 31T 521678 east, 4687224 north.

CC08 Metapelite (46.8% biotite, 25.6% quartz, 16.1% feldspar, 4.2% chlorite, accessory muscovite, ilmenite and tourmaline). Cala Prona, UTM 31T 521678 east, 4687224 north.

CC11a–c pure vein Qtz, sampled along dragged quartz vein. Increasing D3 overprint from CC11a to CC11c. Cala Serena, UTM 31T 521835 east, 4687155 north.

CC14 Metapsammite (44.4% quartz, 25.5% biotite, 20.5% feldspar, 3.5% muscovite, accessory ilmenite, chlorite and tourmaline). Cala Serena, UTM 31T 521859 east, 4687052 north.

CC17a Metapsammite (44.5% quartz, 24.4% feldspar, 23% biotite, 6% muscovite, accessory garnet, ilmenite, chlorite, apatite and tourmaline). Cala Serena, UTM 31T 521968 east, 4686922 north.

CC33a–e pure vein Qtz, sampled along dragged quartz vein, increasing D3 overprint. Cala Serena, UTM 31T 521813 east, 4686788 north.

C37 Metapsammite (49.4% quartz, 30.9% biotite, 14% feldspar, 1.6% muscovite, accessory ilmenite, chlorite and tourmaline). Cala Prona, UTM 31T 521678 east, 4687224 north.

CC52 Metapelite (35.0% quartz, 33.1% biotite, 26.3% feldspar, 6.6% muscovite). Cala Serena, UTM 31T 521911 east, 4686934 north.

References

Anders, M.H., Wiltschko, D.V., 1994. Microfracturing, paleostress and the growth of faults. Journal of Structural Geology 16 (6), 795–815.

Atkinson, B.K., 1982. Subcritical crack propagation in rocks: theory, experimental result and applications. Journal of Structural Geology 4 (1), 41–56.

Atkinson, B.K., Meredith, P.G., 1986. The theory of subcritical crack growth with application to minerals and rocks. In: Atkinson (Ed.), Fracture Mechanics of Rocks. Academic Press.

Bakker, R.J., Jansen, J.B., 1990. Preferential water leakage from fluid inclusions by means of mobile dislocations. Nature 345 (6270), 58–60.

Bakker, R.J., Jansen, J.B., 1994. A mechanism for preferential H_2O leakage from fluid inclusions in quartz, based on tem observations. Contributions to Mineralogy and Petrology 116 (1–2), 7–20.

Barnett, R.L., Kerrich, R., 1980. Stress corrosion cracking of biotite and feldspar. Nature 283, 185–187.

Boullier, A.M., 1999. Fluid inclusions: tectonic indicators. Journal of Structural Geology 21 (8–9), 1229–1235.

Brantley, S.L., 1992. The effect of fluid chemistry on quartz microcrack lifetimes. Earth and Planetary Science Letters 113, 145–156.

Bucher, K., Frey, M., 1994. Petrogenesis of Metamorphic Rocks, sixth ed. Springer, Berlin.

Buergmann, R., Pollard, D.D., 1992. Influence of the state of stress on the brittle–ductile transition in granitic rock: evidence from fault steps in the Sierra Nevada, California. Geology 20, 645–648.

Carreras, J., 2001. Zooming on Northern Cap de Creus shear zones. Journal of Structural Geology 23 (9), 1457–1486.

Carreras, J., Garcia-Celma, A., 1982. Quartz c-axis fabric variation at the margins of a shear zone developed in schists from Cap de Creus (Spain). Acta Geologica Hispanica 17, 137–149.

Carreras, J., Estrada, A., White, S., 1977. The effect of folding on the c-axis fabrics of a quartz mylonite. Tectonophysics 39, 3–24.
Druguet, E., 2001. Development of high thermal gradients by coeval transpression and magmatism during the Variscan orogeny: insights from the Cap de Creus (Eastern Pyrenees). Tectonophysics 332 (1–2), 275–293.
Drury, M.R., Urai, J.L., 1990. Deformation-related recrystallization processes. Tectonophysics 172, 235–253.
Elliott, D., 1976. Energy-balance and deformation mechanisms of thrust sheets. Philosophical Transactions of the Royal Society of London Series A – Mathematical Physical and Engineering Sciences 283 (1312), 289–312.
Fitz Gerald, J.D., Boland, J.N., McLaren, A.C., Ord, A., Hobbs, B.E., 1991. Microstructures in water-weakened single crystals of quartz. Journal of Geophysical Research 96B, 2139–2155.
Fitz Gerald, J.D., Stunitz, H., 1993. Deformation of granitoids at low metamorphic grades. I. Reactions and grainsize reduction. Tectonophysics 221, 269–297.
Fusseis, F., Handy, M.R., Schrank, C., 2006. Networking of shear zones at the brittle-to-viscous transition (Cap de Creus, NE Spain). Journal of Structural Geology 28 (7), 1228–1243.
Fusseis, F., 2006. Strain localization and shear zone formation at the brittle–viscous transition, Cap de Creus, Spain. Published PhD thesis, Freie Universität Berlin, Germany, http://www.diss.fu-berlin.de/2007/67/indexe.html.
Garcia-Celma, A., 1983. C-axis and shape fabrics in quartz mylonites of Cap de Creus (Spain): their properties and development. Unpublished Ph.D. thesis, University of Utrecht.
Ghandi, C., Ashby, M.F., 1979. Fracture-mechanism maps for materials which cleave – F.C.C., B.C.C. and H.C.P. metals and ceramics. Acta Metallurgica 27, 1565–1602.
Guermani, A., Pennacchioni, G., 1998. Brittle precursors of plastic deformation in a granite: an example from the Mont Blanc massif (Helvetic, western Alps). Journal of Structural Geology 20 (2–3), 135–148.
Henry, D.J., Guidotti, C.V., 2002. Ti in biotite from metapelitic rocks: temperature effects, crystallochemical controls and petrologic applications. American Mineralogist 87, 375–382.
Henry, D.J., Guidotti, C.V., Thomson, J.A., 2005. The Ti-saturation surface for low-to-medium pressure metapelitic biotite: implications for geothermometry and Ti-substitution mechanisms. American Mineralogist 90, 316–328.
Herwegh, M., Handy, M.R., 1996. The evolution of high-temperature mylonitic microfabrics: evidence from simple shearing of a quartz analogue (norcamphor). Journal of Structural Geology 18 (5), 689–710.
Hull, J., 1988. Thickness-displacement relationships for deformation zones. Journal of Structural Geology 10, 244–267.
Ingles, J., 1986. Terminations of ductile shear zones. Tectonophysics 127, 87–95.
Ji, S., Mainprice, D., 1988. Natural deformation fabrics of plagioclase: implications for slip systems and seismic anisotropy. Tectonophysics 147 (1–2), 145–163.
Kerrich, R., 1976. Some effects of tectonic recrystallization on fluid inclusions in vein quartz. Contributions to Mineralogy and Petrology 59, 192–202.
Kerrich, R., Allison, I., Barnett, R.L., Moss, S., Starkey, J., 1980. Microstructural and chemical-transformations accompanying deformation of granite in a shear zone at Mieville, Switzerland – with implications for stress-corrosion cracking and superplastic flow. Contributions to Mineralogy and Petrology 73 (3), 221–242.
Kerrich, R., Latour, T.E., Barnett, R.L., 1981. Mineral reactions participating in intragranular fracture propagation – implications for stress-corrosion cracking. Journal of Structural Geology 3 (1), 77–87.
Kirby, S.H., McCormick, J.W., 1979. Creep of hydrolytically weakened synthetic quartz crystals oriented to promote {2110}⟨001⟩slip: a brief summary of work to date. Bulletin de Mineralogie 102, 124–137.
Kohlstedt, D., 2006. The role of water in high-temperature rock deformation. Reviews in Mineralogy and Geochemistry 62, 377–396.
Kruse, R., Stunitz, H., Kunze, K., 2001. Dynamic recrystallization processes in plagioclase porphyroclasts. Journal of Structural Geology 23 (11), 1781–1802.
Lespinasse, M., 1999. Are fluid inclusion planes useful in structural geology? Journal of Structural Geology 21 (8–9), 1237–1243.
Mancktelow, N.S., Pennacchioni, G., 2005. The control of precursor brittle fracture and fluid-rock interaction on the development of single and paired ductile shear zones. Journal of Structural Geology 27 (4), 645–661.
March, A., 1932. Mathematische Theorie der Regelung nach Korngestalt bei Affiner Deformation. Zeitschrift für Kristallographie 81, 285–297.
McLaren, A.C., Fitz Gerald, J.D., Gerretsen, J., 1989. Dislocation nucleation and multiplication in synthetic quartz: relevance to water weakening. Physics and Chemistry of Minerals 16, 465–482.
McLaren, A.C., Pryer, L.L., 2001. Microstructural investigation of the interaction and interdependence of cataclastic and plastic mechanisms in feldspar crystals deformed in the semi-brittle field. Tectonophysics 335, 1–15.
Means, W.D., 1984. Shear zones of types I and II and their significance for the reconstruction of rock history. Geological Society of America Bulletin. Abstract Programs 16, 50.
Means, W.D., 1995. Shear zones and rock history. Tectonophysics 247, 157–160.
Mitra, G., 1979. Ductile deformation zones in blue ridge basement rocks and estimation of finite strains. Geological Society of America Bulletin 90 (10), 935–951.
Mitra, G., 1984. Brittle to ductile transition due to large strains along the white rock thrust, wind river mountains, Wyoming. Journal of Structural Geology 6 (1–2), 51–61.
Newman, J., Lamb, W.M., Drury, M.R., Vissers, R.L.M., 1999. Deformation processes in a peridotite shear zone: reaction-softening by an H_2O-deficient, continuous net transfer reaction. Tectonophysics 303 (1–4), 193–222.
Nyman, M.W., Law, R.D., Smelik, E.A., 1992. Cataclastic deformation mechanism for the development of core-mantle structures in amphibole. Geology 20 (5), 455–458.
Passchier, C.W., Trouw, R.A.J., 2005. Microtectonics. Springer. 366p.
Paterson, M.S., 1989. Interaction of water with quartz and its influence in dislocation flow: an overview. In: Karato, S.-i., Toriumi, M. (Eds.), Rheology of Solids and of the Earth. Oxford University Press, pp. 107–142.
Pennacchioni, G., 2005. Control of the geometry of precursor brittle structures on the type of ductile shear zone in the Adamello tonalites, Southern Alps (Italy). Journal of Structural Geology 27 (4), 627–644.
Poirier, J.P., 1980. Shear localization and shear instability in materials in the ductile field. Journal of Structural Geology 2 (1–2), 135–142.
Ramsay, J.G., 1980. Shear zone geometry: a review. Journal of Structural Geology 2 (1/2), 83–99.
Ramsay, J.G., Allison, I., 1979. Structural analysis of shear zone in an alpinised Hercynian granite (Maggia Lappen, Pennine Zone, Switzerland). Schweizer Mineralogische und Petrographische Mitteilungen 59, 251–279.
Schmid, S.M., Handy, M.R., 1991. Towards a genetic classification of fault rocks: geological usage and tectonophysical implications. In: Muller, D.W., McKenzie, J.A., Weissert, H. (Eds.), Controversies in Modern Geology: Evolution of Geological Theories in Sedimentology, Earth History and Tectonics. Academic Press, London.
Schrank, C., Handy, M.R., Fusseis, F., in press. Multiscaling of shear zones and the evolution of the brittle-to-viscous transition in continental crust. Journal of Geophysical Research.
Segall, P., Pollard, D., 1983. Nucleation and growth of strike slip faults in granite. Journal of Geophysical Research 88 (B1), 555–568.
Segall, P., Simpson, C., 1986. Nucleation of ductile shear zones on dilatant fractures. Geology 14 (1), 56–59.
Shea, W.T., Kronenberg, A.K., 1992. Rheology and deformation mechanisms of an isotropic mica schist. Journal of Geophysical Research 97 (B11), 15201–15237.
Shea, W.T., Kronenberg, A.K., 1993. Strength and anisotropy of foliated rocks with varied mica contents. Journal of Structural Geology 15 (9–10), 1097–1121.
Simpson, C., 1983. Displacement and strain patterns from naturally occurring shear zone terminations. Journal of Structural Geology 5 (6), 497–506.
Simpson, C., 1986. Fabric development in brittle-to-ductile shear zones. Pure and Applied Geophysics 124 (1–2), 269–288.
Stipp, M., Stunitz, H., Heilbronner, R., Schmid, S.M., 2002. The eastern Tonale fault zone: a 'natural laboratory' for crystal plastic deformation of quartz over a temperature range from 250 to 700 °C. Journal of Structural Geology 24 (12), 1861–1884.
Stunitz, H., Fitz Gerald, J.D., 1993. Deformation of granitoids at low metamorphic grade. II: granular flow in albite-rich mylonites. Tectonophysics 221, 299–324.
Stunitz, H., Fitz Gerald, J.D., Tullis, J., 2003. Dislocation generation, slip systems and dynamic recrystallization in experimentally deformed plagioclase single crystals. Tectonophysics 372, 215–233.
Tourigny, G., Tremblay, A., 1997. Origin and incremental evolution of brittle/ductile shear zones in granitic rocks: Natural examples from the southern Abitibi Belt, Canada. Journal of Structural Geology 19 (1), 15–27.
Trepmann, C.A., Stöckhert, B., Dorner, D., Moghadam, E.H., Küster, M., Röller, K., 2007. Simulatinf coseismic deformation of quartz in the middle crust and fabric evolution during postseismic stress relaxation – an experimental study. Tectonophysics 442, 83–104.
Tullis, J., Yund, R.A., 1980. Hydrolytic weakening of experimentally deformed Westerly Granite and Hale albite rock. Journal of Structural Geology 2, 439–451.
Urai, J.L., 1983. Water assisted dynamic recrystallization and weakening in polycrystalline bischofite. Tectonophysics 96 (1–2), 125–157.
Urai, J.L., Spiers, C.J., Zwart, H.J., Lister, G.S., 1986. Weakening of rock salt by water during long-term creep. Nature 324 (6097), 554–557.
van Daalen, M., Heilbronner, R., Kunze, K., 1999. Orientation analysis of localized shear deformation in quartz fibres at the brittle–ductile transition. Tectonophysics 303 (1–4), 83–107.
Vernooij, M.G.C., Kunze, K., den Brok, B., 2006. 'Brittle' shear zones in experimentally deformed quartz single crystals. Journal of Structural Geology 28 (7), 1292–1306.
Watterson, J., 1986. Fault dimensions, displacement and growth. PAGEOPH 124 (1/2), 365–373.
White, S.H., 1976. The role of dislocation processes during tectonic deformation with special reference to quartz. In: Strens, R.J. (Ed.), The Physics and Chemistry of Minerals and Rocks. Wiley, London, pp. 75–91.
White, S., 1977. Geological significance of recovery and recrystallization processes in quartz. Tectonophysics 39 (1–3), 143–170.
White, S., Burrows, S.E., Carreras, J., Shaw, N.D., Humphreys, F.J., 1980. On mylonites in ductile shear zones. Journal of Structural Geology 2 (1–2), 175–187.
Wilkins, R.W.T., Barkas, J.P., 1978. Fluid inclusions, deformation and recrystallization in granite tectonics. Contributions to Mineralogy and Petrology 65 (3), 293–299.